

The dependence of the biodegradable ZX10 alloy corrosion process on the structural factors and local pH level

© 2023

Pavel N. Myagkikh^{*1}, junior researcher of the Research Institute of Advanced Technologies

*Evgeny D. Merson*², PhD (Physics and Mathematics),

senior researcher of the Research Institute of Advanced Technologies

*Vitaly A. Poluyanov*³, PhD (Engineering),

junior researcher of the Research Institute of Advanced Technologies

*Dmitry L. Merson*⁴, Doctor of Sciences (Physics and Mathematics), Professor,

Director of the Research Institute of Advanced Technologies

Togliatti State University, Togliatti (Russia)

*E-mail: feanorhao@gmail.com,
p.myagkikh@tltsu.ru

¹ORCID: <https://orcid.org/0000-0002-7530-9518>

²ORCID: <https://orcid.org/0000-0002-7063-088X>

³ORCID: <https://orcid.org/0000-0002-0570-2584>

⁴ORCID: <https://orcid.org/0000-0001-5006-4115>

Received 18.05.2023

Accepted 29.05.2023

Abstract: Magnesium biodegradable alloys are a promising material for self-dissolving surgical implants. Magnesium is known to be sensitive to electrochemical corrosion due to the galvanic effect between the matrix and particles of secondary phases and inclusions. Another important factor is the pH level. The behavior of certain chemical reactions depends on the pH level, so one can assume that the pH level of a corrosive medium at the material surface is a factor determining what chemical reactions can occur there. Finally, there is evidence that variability of the crystallographic orientation of the grains may be a cause of anisotropy of corrosion properties. The purpose of this work is to reveal the influence of the electrode potential of the microstructural elements, the crystallographic orientation of the grains, and the pH level of the near-surface volume of the corrosion solution on the corrosion process. In the study, sections of 2×1.5 mm were marked on the ZX10 alloy samples, for which maps of the distribution of crystallographic orientations and chemical composition were drawn. To assess the influence of the electrode potential of the particles, the authors carried out a Kelvin probe mapping in the 90×90 μm area. Next, corrosion tests were carried out with video filming of the surface on the marked area. To determine the pH level influence, the solution circulation in the cell was varied. Upon completion of the tests, corrosion products and corrosion damage were examined in detail. According to the results, the pH level in the liquid near-surface micro-volumes has a greater influence than the electrode potential of the particles as it provokes the formation of corrosion products of a different composition, which leads to passivation of the surface areas around the particles. The authors identified two different types of filiform corrosion. For filiform corrosion, a correlation between the corrosion direction and the crystallographic orientation of the grains was established.

Keywords: magnesium alloys; corrosion; ZX10; biodegradable materials; medical implants; electrode potential; pH level; crystallography; filiform corrosion.

Acknowledgments: The research was financially supported by the Russian Science Foundation, project No. 23-23-10041.

The paper was written on the reports of the participants of the XI International School of Physical Materials Science (SPM-2023), Togliatti, September 11–15, 2023.

For citation: Myagkikh P.N., Merson E.D., Poluyanov V.A., Merson D.L. The dependence of the biodegradable ZX10 alloy corrosion process on the structural factors and local pH level. *Frontier Materials & Technologies*, 2023, no. 2. DOI: 10.18323/2782-4039-2023-2-64-3.

INTRODUCTION

Traditionally, stainless steels and titanium-based alloys are used to produce surgical implants, such as screws for fixing bone fragments and plates for osteosynthesis. Upon completion of the healing process, in most cases, these implants are to be removed. The removal operation has a number of negative effects: risks for the patient's health, the need for post-operative recovery, an increase in the patient's disability period, etc. Therefore, one of the promising areas in this field is the creation of self-dissolving (biodegradable) metal implants. One of the most suitable metals for this purpose is magnesium: an important role in human metabolism and low cytotoxicity ensure its good biocompatibility, and mechanical characteristics close to bone tissues guarantee mechanical compatibility [1]. Since the metal dissolution in the human body is nothing but corrosion,

the study of the mechanisms of corrosion processes in magnesium alloys is of great importance for both fundamental and applied science. Several factors significantly affecting the corrosion of magnesium alloys are known.

The variability of the grain crystallographic orientation can cause anisotropy of corrosion properties [2], as well as a tendency to filiform corrosion [3]. However, the experiments carried out on single crystals and polycrystals with coarse grains show contradictory results: in the work [3], it was identified that the basal plane (0001) exhibits the lowest corrosion resistance, while the works [4; 5] indicate that such an orientation of crystallites, on the contrary, provides the highest corrosion resistance. In the case of a fine-grained polycrystal, crystallographic texture has a great influence on corrosion, a phenomenon often observed after extrusion, rolling, or other thermomechanical processing of magnesium alloys, and consisting in the predominance of

a certain orientation in most semi-finished product crystallites. In the work [6], when studying the anisotropy of the extruded magnesium corrosion properties, it was identified that the section plane along the bar with the predominant grain orientation (0001) is much more corrosion resistant than the plane in the section across the bar. Thus, the influence of crystallography can play an important role in the corrosion processes of magnesium alloys.

The particles of secondary phases and inclusions are equally important. Magnesium has an electrode potential of -2.375 V [7], which is significantly lower than that of most metals used as alloying elements in magnesium alloys. This causes its tendency to electrochemical corrosion manifesting itself during the interaction in a corrosive environment between two metals with different potentials. Since, under the galvanic effect, the material with a more negative potential is dissolved first, most of the particles, being positive with respect to magnesium, reduce the material corrosion resistance by provoking an intensive dissolution of the magnesium matrix.

Speaking about the particles with a more negative electron potential than magnesium, one should keep in mind several factors. First, as shown in [8], phases with a more negative potential compared to the matrix can form corrosion products, which, on the contrary, play the role of a cathode. Second, it is necessary to take into account the change in the electrode potentials of the matrix and, the secondary phase under the action of alloying elements in the form of a solid solution. It is known that many elements, such as zinc and silver [7], increase the potential of the magnesium matrix when forming a solid solution. The dissolution of such elements in secondary phases, for example, in the Mg_2Ca intermetallic compound, which has a more negative electrode potential than magnesium, leads to a shift in their potential to more positive values. The work [9] indicates that when the zinc concentration exceeds the value of 1.07 %, the Mg_2Ca phase becomes more positive than the matrix. Finally, one must take into account the fact, that the dissolution of a particle even more negative than the matrix will change the pH level in the corrosive medium microvolumes near the sample surface.

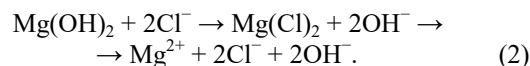
The primary reaction of magnesium in media simulating human body fluids, such as NaCl saline 0.9 %, Ringer's solution, Hanks' solution, etc., is as follows:



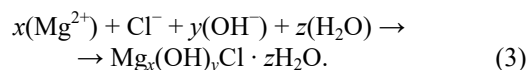
The magnesium hydroxide produced during the reaction is a weak, poorly soluble base and performs two functions: to some extent passivates the material surface and, by dissociating into a magnesium cation and a hydroxyl group anion, increases the pH level. According to [8], the Mg_2Ca phase reacts with water in a similar reaction to form magnesium hydroxide and calcium hydroxide, which is a strong base. It follows from this that the corrosion of particles of such secondary phases as Mg_2Ca can lead to a significant local increase in the pH level. Based on the Pourbaix diagrams for pure magnesium in water presented in [10; 11], one can conclude that under conditions of a certain electrode potential of the surface and the pH level, various compounds can be stable: oxide, hydride, magnesium hydroxide, as well as magnesium itself, i.e., depending on the

electrode potential and the pH level, the flow of well-defined reactions are thermodynamically favorable. This means that changing the pH level can significantly affect the type of corrosion products formed when reacting with water.

In solutions containing chloride ions, the reaction described by formula (1) may continue in the form of a reaction of chlorine anion with hydroxide:



As can be seen from the reaction equation, chlorine contributes to the destruction of magnesium hydroxide, which plays the role of a weak passivating film, and then the well-soluble magnesium chloride formed can dissociate in water into magnesium and chlorine ions. However, due to the influence of various factors, such as the concentration of some ions in the solution, reactions that are more complex can occur, for example, the reaction with the formation of oxychlorides described in [8]:



Detailed information on the formation of various oxychlorides in aqueous solutions at 23 °C is presented in the work [12]. The authors indicate that mainly two types of oxychlorides are formed: $5Mg(OH)_2 \cdot MgCl_2 \cdot 8H_2O$ (shortly 5·1·8) and $3Mg(OH)_2 \cdot MgCl_2 \cdot 8H_2O$ (shortly 3·1·8), noting that these compounds differ significantly: 5·1·8 is formed faster, and 3·1·8 tends to react with carbon dioxide and carbonate ions with the formation of chlorocarbonate. The conditions for the formation of compounds also differ from each other and depend on the concentration of chloride ions and the pH level.

Following all this, one can draw the conclusion: the electrode potential determines what will be destroyed first of all – a particle of secondary phases and inclusions or a matrix, and the pH level in the microvolumes of the corrosive medium near the metal surface, affects what chemical reactions will take place. However, it is not clear which of these factors is more important, especially against the background of the matrix crystallographic effect. Determining the influence of all three factors is important for understanding the mechanism of corrosion processes and, therefore, predicting the corrosion properties of materials and the efficiency of thermal and thermomechanical treatment modes.

The aim of this work is to study the influence of the crystallographic orientation of grains, secondary phase particles, as well as the pH level in microvolumes of the corrosive medium near the sample surface on the corrosion process of the biodegradable ZX10 alloy.

METHODS

A biodegradable as-cast ZX10 alloy of the Mg–Zn–Ca system was chosen for the study. This alloy has good cytotoxicity characteristics [13], high strength properties [14], and a relatively low corrosion rate [1; 14]. The exact chemical composition was determined using a Thermo Fisher Scientific ARL 4460 OES optical emission spectrometer.

The samples were rectangular plates of 30×15×1 mm ground on #2500 sandpaper. After grinding, in the middle of the right half of one of the sample surfaces, a 2×1.5 mm area was marked with a hard-tip chisel for precision research. Then, the surface with the marked area was polished on anhydrous diamond suspensions with an abrasive size of 3, 1, and 0.25 μm in succession. After that, the marked area was subjected to ion polishing in a Hitachi IM4000Plus device. Treatment was carried out in an ionized argon beam at an angle of 5° to the sample surface for 35 min at an accelerating voltage of 3.2 kV. From the marked area, a distribution map of crystallographic orientations was taken in the column of a Carl Zeiss SIGMA scanning electron microscope (SEM) using an EDAX module for analyzing electron back-scattered diffraction (EBSD). In the SEM column, mapping was also carried out with determining the elemental composition on the surface of the marked area using energy dispersive spectrometry (EDS). On the surface of the sample marked area intended to identify the role of the electrode potential (hereinafter, this sample is marked as EP), an area of 90×90 μm with several particles was selected, and in this area, an electrode potential distribution map was taken according to the Kelvin probe method using a NT-MDT Solver NEXT atomic force microscope. Further, all samples were subjected to corrosion tests.

The tests included holding the sample for 24 h in Ringier's solution with the composition of 8.36 g NaCl, 0.3 g KCl, 0.15 g CaCl₂ per 1000 ml of water. The corrosion cell volume was 5 l. The sample was fixed vertically in a silicone clamp in such a way that the clamp was as far as possible from the marked area. To monitor corrosion processes, a camera was directed to the area marked with a chisel, by analogy with our previous work [15]. Video surveillance during corrosion tests is an *in situ* method that allows tracking the staging of the corrosion damage appearance and the dynamics of their development. This method showed good results when studying the dependence of the direction of filiform corrosion propagation on the crystallographic grain orientation [16]. When testing a sample intended to determine the pH influence (hereinafter marked as PH), the corrosive medium was circulated using a peristaltic pump. The tube, through which the corrosive solution was pumped into the corrosion cell, was directed straight to the marked area from below, so that the flow was oriented diagonally from the lower right corner of the marked area tangentially to the sample surface. Thus, the corrosive medium at the sample surface, the pH level of which could be increased due to the occurrence of corrosion processes, was washed away by the solution flow.

After completion of the tests, the samples were removed, dried in a fore vacuum at room temperature for 2 h, and then loaded into a SEM to map the distribution of chemical elements in corrosion products. Then the corrosion products were removed by immersion in an aqueous solution of 20 % CrO₃+1 % AgNO₃ for 1 min by analogy with the work [17]. When removing corrosion products, a Sapphire ultrasonic bath was used. After the removal of corrosion products, the corrosion damage depth and morphology were assessed using an Olympus Lext OLS4000 confocal laser scanning microscope (CLSM).

RESULTS

Table 1 presents the ZX10 alloy chemical composition.

Fig. 1 shows a map of the distribution of crystallographic orientations, as well as of particles of secondary phases, and inclusions in the marked area of the EP sample. Fig. 2 shows maps of the distribution of the electrode potential and chemical elements in the area marked with a rectangle in Fig. 1. The area contains three large particles with different chemical compositions and electrode potentials. Particles No. 1 and 3 are clearly oxidized, presumably due to the air contact.

Fig. 3 presents a storyboard of the video recording of the EP sample corrosion tests. The location of corrosion centres correlates well with the distribution maps of chemical elements in Fig. 1. The structure is visible only during the first 2 h of the experiment, after which the grain boundaries become practically invisible. In 12 h, typical pale regions form around all the observed particles in the marked area due to the formation of corrosion products. No dependence of the corrosion process occurrence on grain orientation is observed. After 12 h of testing, filiform corrosion traces appear in the corner of the marked area (indicated by a red arrow), but their subsequent growth does not occur.

Fig. 4 shows a map of crystallographic orientations, and distribution of particles of secondary phases and inclusions in the marked area of the PH sample.

Fig. 5 shows a storyboard of video recording of the PH sample corrosion test. From the very beginning of the test until its completion, the structure is clearly visible, the sample remains shiny for all 24 h and is not covered with a dense layer of corrosion products, corrosion centres are clearly visible, but wide zones covered with corrosion products do not form around them. After 23 h of testing, filiform corrosion traces become visible. One should note that, as in the case of the EP sample, the initial filiform corrosion spreads along the scratches that marked the area under the study. In both cases, filiform corrosion propagates at a rate of tens or even hundreds of microns per minute.

Fig. 6 demonstrates images of the marked areas of both samples before the removal of corrosion products, as well as a height map taken using CLSM after the corrosion products were removed. Using the height map, it is possible to estimate the depth of filiform corrosion damage, it equals to 10–15 μm.

Fig. 7 shows the surface of the marked areas of both samples with a superimposed map of the distribution of crystallographic orientations. It is evidently that both samples are characterised by the presence of two types of filiform corrosion. Except for the first type damage shown by red arrows in Fig. 3 and 5, after the removal of corrosion products, the second type damage becomes visible in the form of a fine mesh and especially clearly visible on the PH sample.

Fig. 8 presents the maps of the chlorine and oxygen distribution in corrosion products. The EP sample is characterised by the formation of zones significantly depleted in these elements around corrosion centres (i.e., particles of secondary phases and inclusions). This confirms the assertion, based on the obtained height maps that there is practically no corrosion in these places. There is a lot of zinc in corrosion products, both in the form of inclusions and evenly distributed over the surface. Calcium and zirconium are present mainly in the form of inclusions; the concentration of both elements in the corrosion products is less than 0.1 %.

Table 1. Chemical composition of the ZX10 alloy, % wt.

Mg	Zn	Zr	Ca	Fe	Mn	Si	Al	Cu
Base	0.84	0.03	0.17	<0.004	0.007	0.008	0.01	<0.001

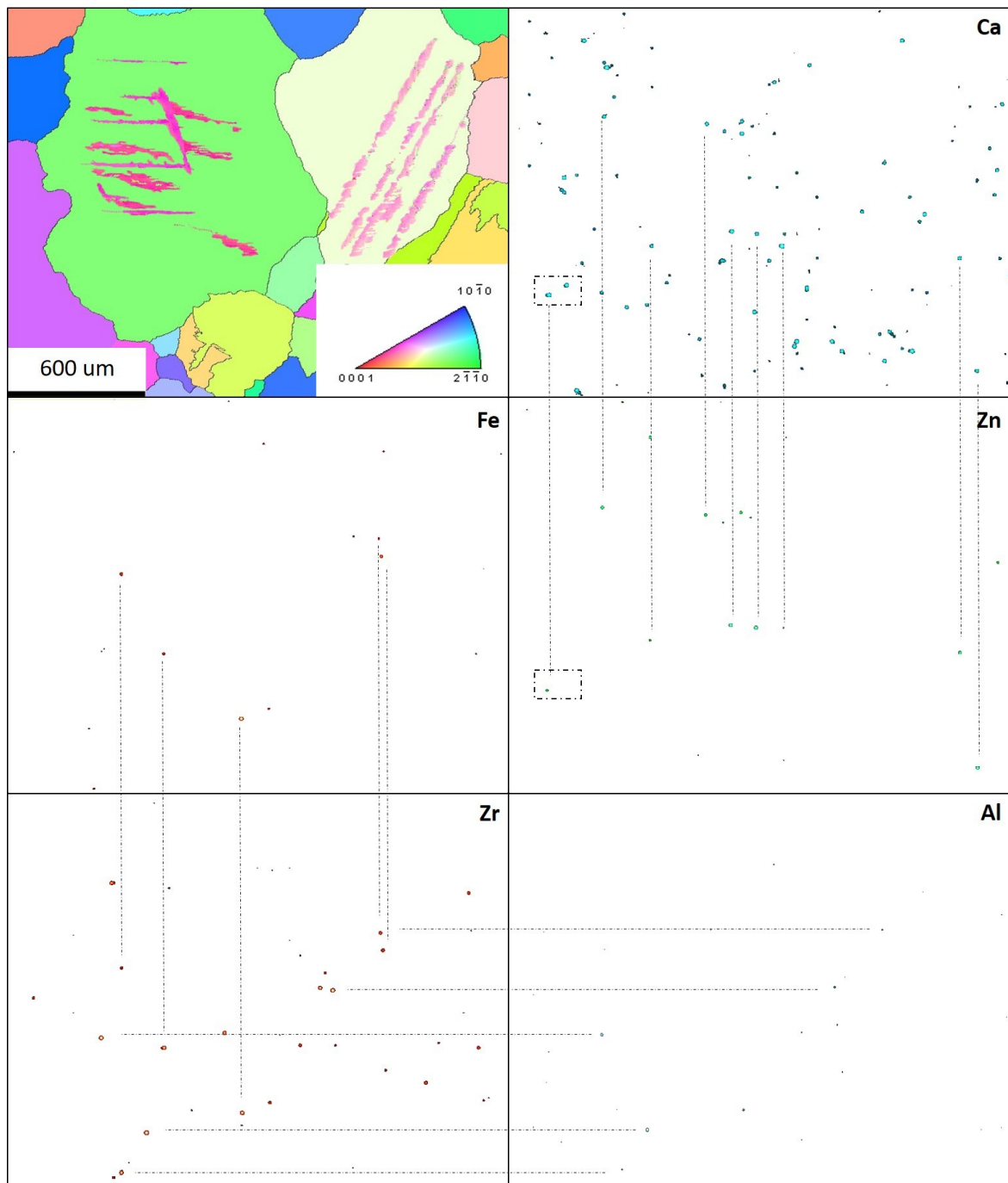


Fig. 1. IPF-map and mapping of the particles of secondary phases and inclusions on the marked surface of EP-sample (the lines connect the same particles on the maps of different elements)

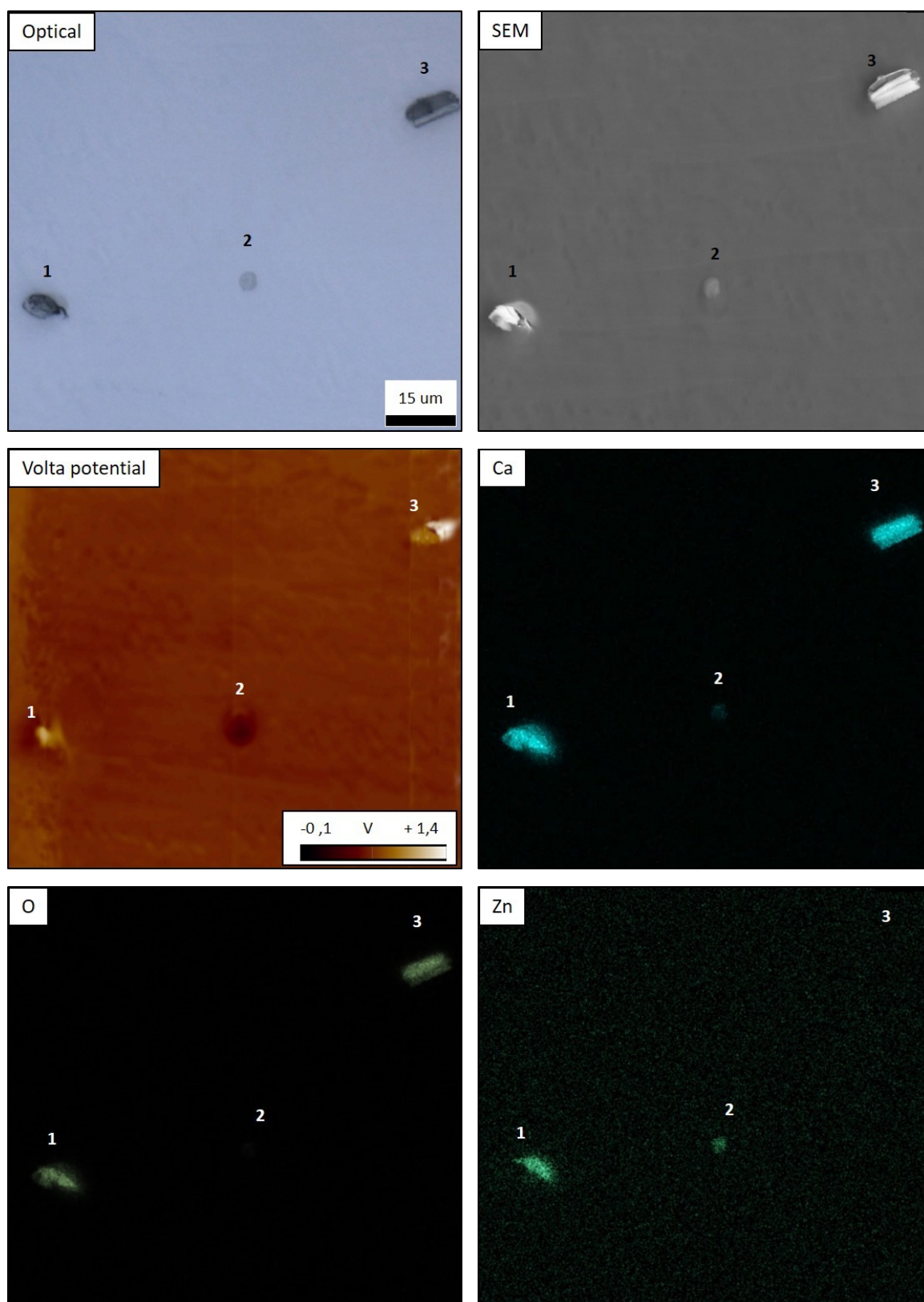


Fig. 2. Volta potential map (by Kelvin probe method) and chemical composition of the particles in the rectangular area highlighted on the maps of zinc and calcium distribution in Fig. 1

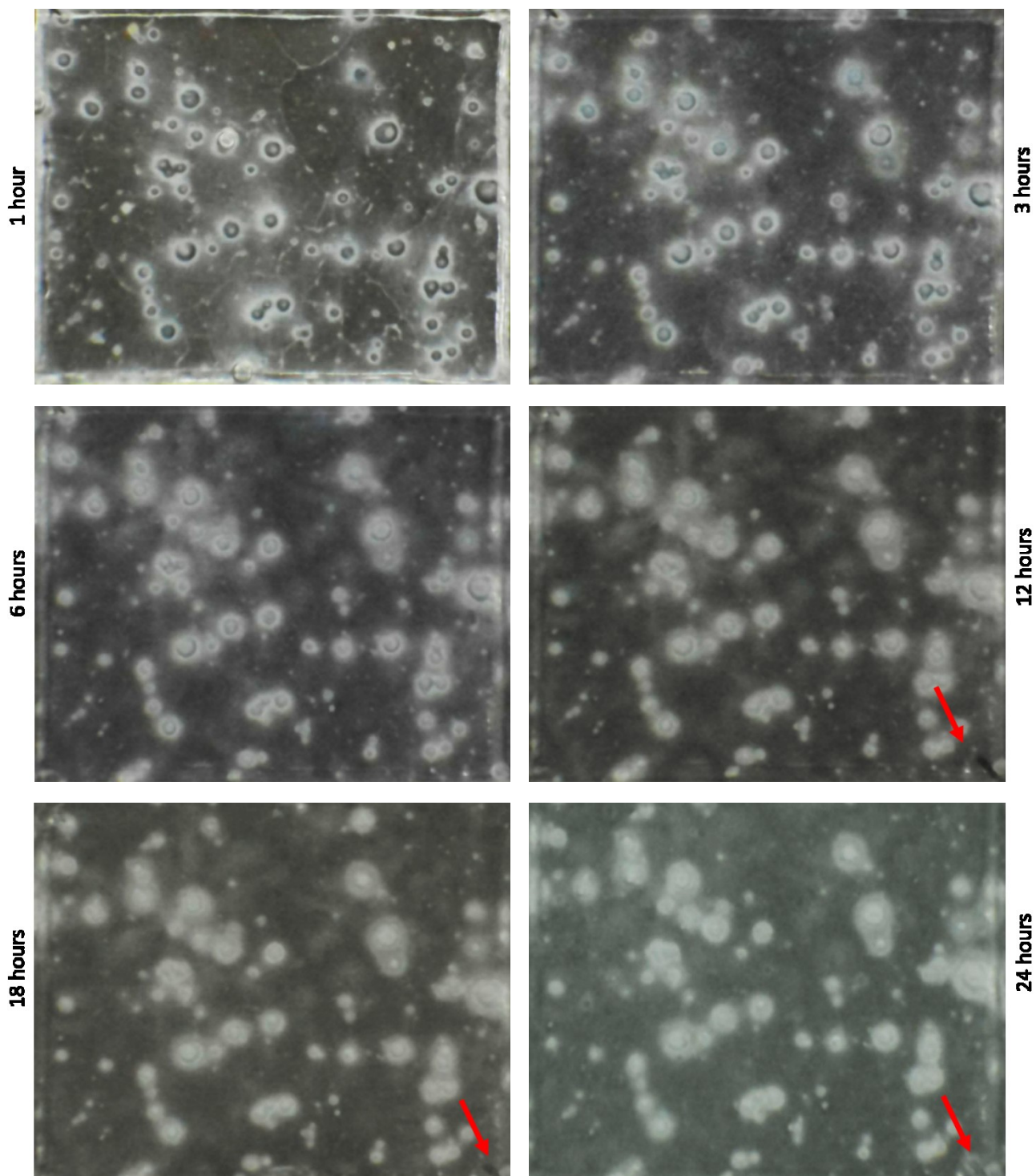


Fig. 3. Video-monitoring results of the EP-sample marked surface during the corrosion test. Red arrows indicate filiform corrosion

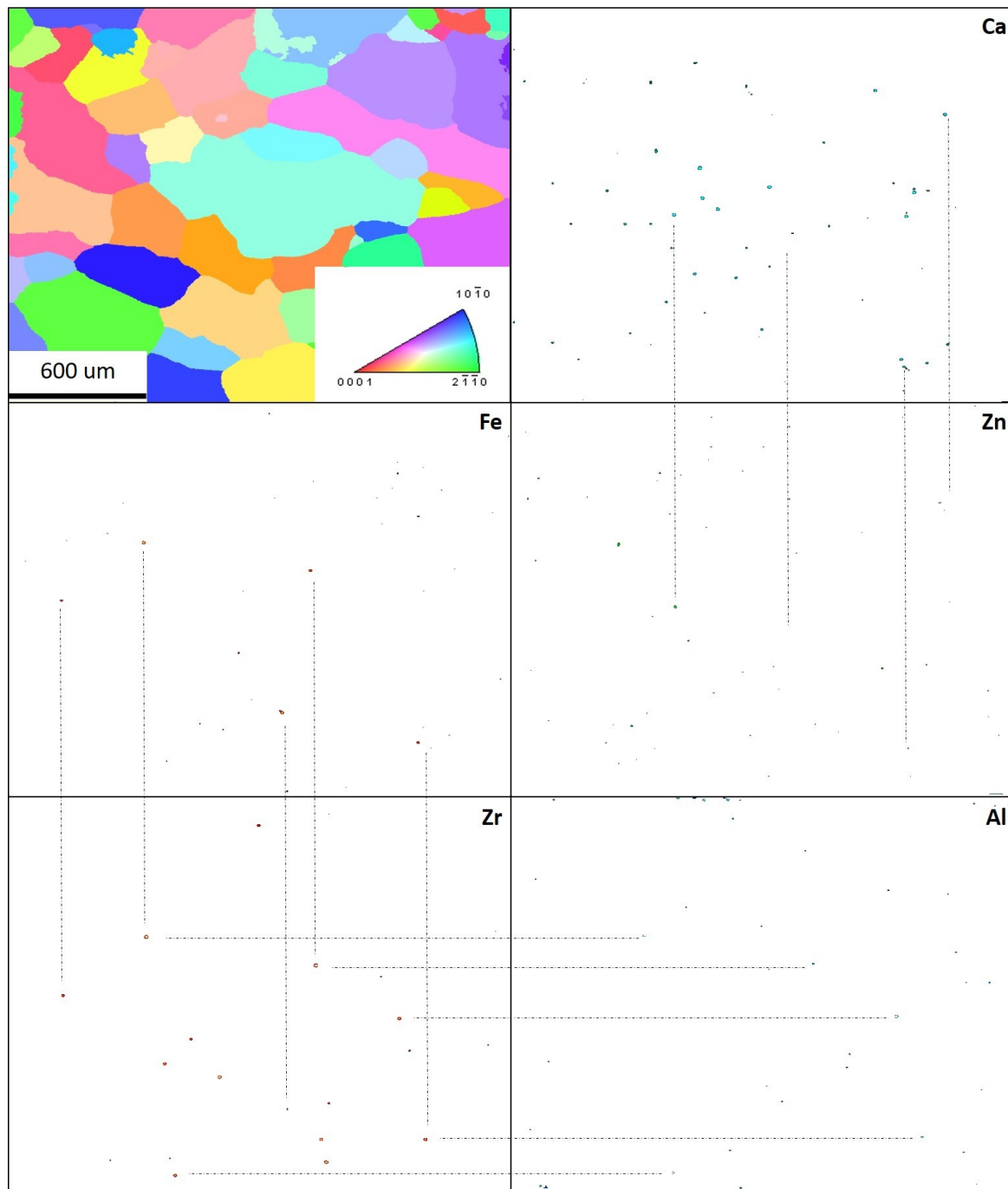


Fig. 4. IPF-map and mapping of the particles of secondary phases and inclusions on the marked surface of the pH-sample

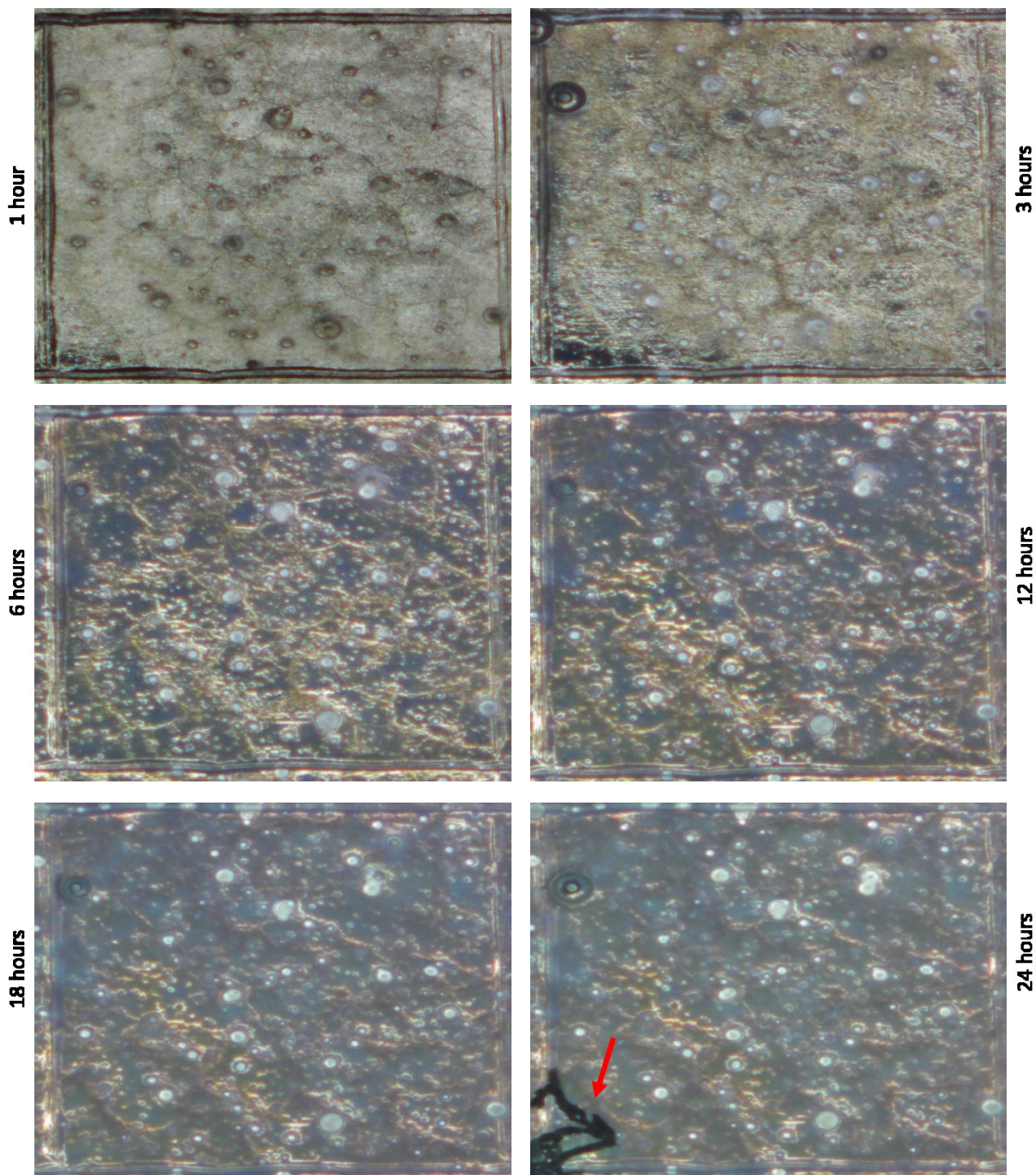


Fig. 5. The results of video-monitoring of the marked surface of the pH-sample during corrosion test. Red arrow indicates filiform corrosion

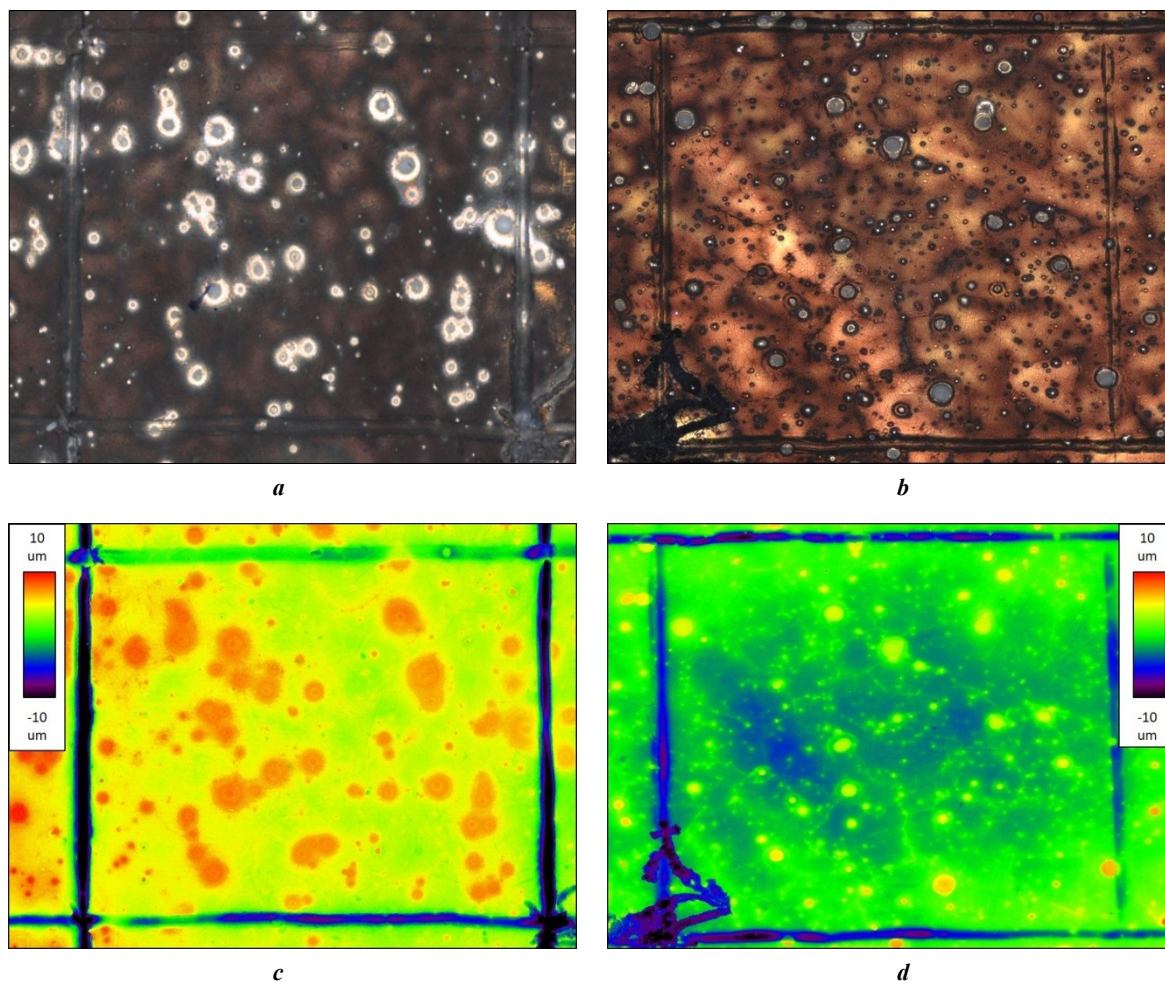


Fig. 6. Images of marked areas of samples to reveal the role of the electrode potential (EP) (a, c) and to determine the pH (PH) effect (b, d):

a, b – before the removal of corrosion products (optical microscopy);
c, d – after the removal of corrosion products (height map obtained using CLSM)

The PH sample pattern looks completely different (Fig. 9). Around the corrosion centres, there are no oxygen-depleted zones; this element is distributed evenly over the entire surface. Chlorine is distributed mainly point-wise, with most of it concentrated at the place of filiform corrosion damage of the first type. For calcium and carbon, the same patterns remain as for EP sample, but the quantity of zirconium and zinc in the corrosion products of the PH sample, are many times greater than in the EP sample corrosion products, and generally in the material. Probably, when magnesium is dissolved, these corrosion-resistant elements remain in the corrosion products.

Fig. 10 shows the maps of heights and distribution of chemical elements in corrosion products in the area shown in Fig. 2. On the height map and the oxygen and chlorine distribution maps, no differences between the particles are visible. In the region of particles No. 1 and 3, their residues in the form of calcium traces are noticeable.

Fig. 11 and 12 present the results of a detailed study of filiform corrosion damage of the first type on the PH specimen. Corrosion spread directionally; there is a large amount of chlorine at the end propagation points and places of change of its direction, although chlorine is not observed over the rest area affected by filiform corrosion. From

Fig. 11 b, it is obvious that this type of corrosion strongly depends on the grain crystallographic orientation, and therefore, changes the direction of its propagation when moving from one grain to another. No correlation between the location of the most chlorine and the deepest damages is observed. The study identified an interesting honeycomb morphology of the walls of the “channel” for the filiform corrosion propagation, which is shown in Fig. 12 e, 12 f. The morphology has the form of rectangular honeycombs oriented across the direction of corrosion propagation. A fragment in Fig. 12 f is located at the boundary of two grains with different orientations. It is seen that along with the propagation direction, in this place, the orientation of the honeycombs also changes by almost 90°. This image also allows estimating the width of the channels of the second type filiform corrosion, which is about 1 µm.

DISCUSSION

Fig. 1 shows that calcium in the particles often adjoins zinc (shown by dotted lines), and there is clearly more zinc in these secondary phases. It is also obvious that there are quite a lot of particles containing calcium, but not containing zinc in the microstructure. Quite likely, these are

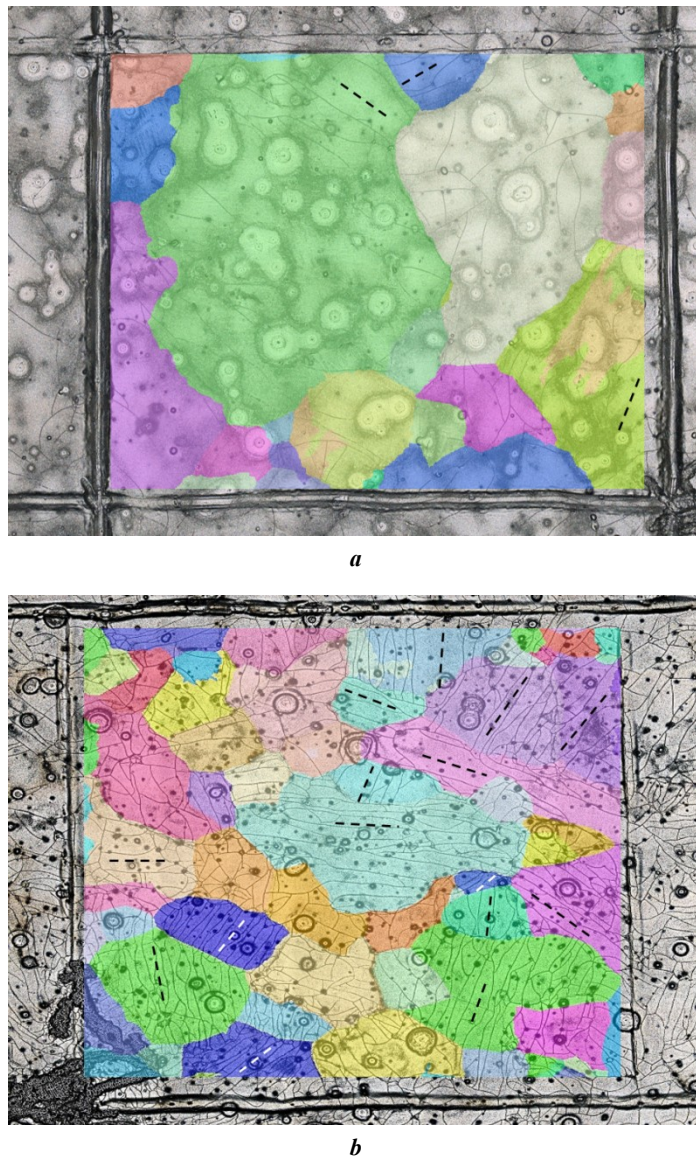


Fig. 7. Images of marked areas of the samples to reveal the role of the electrode potential (EP) (a) and to determine the pH (PH) effect (b) after the removal of corrosion products. A map of the distribution of crystallographic orientations is superimposed on the optical image. The dotted lines show the main direction of second type filiform corrosion

the Mg_2Ca phase particles. Zirconium is adjoins iron and aluminum, with which, as is known, it is capable of forming intermetallic compounds [18]. In the case of iron, due to the transition to the Fe_2Zr intermetallide, its negative effect on corrosion properties is reduced [19]. For the PH sample, the same features of the distribution of particles of secondary phases and inclusions of various compositions are noted as for the EP sample. In Fig. 6, it is clearly seen that a wide rounded zone is formed around the inclusions on the EP sample surface, which, judging by the height map, is subjected to the least corrosion damage. The PH sample is characterized by an elevation in the immediate proximity to a particle; large rounded zones, as in the EP sample, are not observed.

For both samples, the presence of two types of filiform corrosion is noticeable. The first type damage is characterized by a wide channel appearing in scratches and growing in one direction, which, judging by Fig. 7 and 11, has a dependence on grain orientation. The second type damage

is very thin, covering the entire marked area with a fine mesh. Initially, a hypothesis arose that these damages were associated with cracking of the crust of corrosion products and the corrosion medium penetration, under the passivating layer. However, comparison with the grain orientation map clearly indicates that the direction of the filiform corrosion propagation depends on the crystallographic orientation, while, in the case of corrosion product cracking, the directions should have been chaotic. An interesting fact is that the PH sample has much more damages of this type and their correlation with crystallography can be traced significantly better than that of the EP sample. On the PH sample, it can also be observed, that on the grains with an orientation close to (0001), there is no predominant direction for filiform corrosion traces, while they are usually parallel to each other on the grains of different orientations. However, considering the small sample size, this observation needs to be clarified.

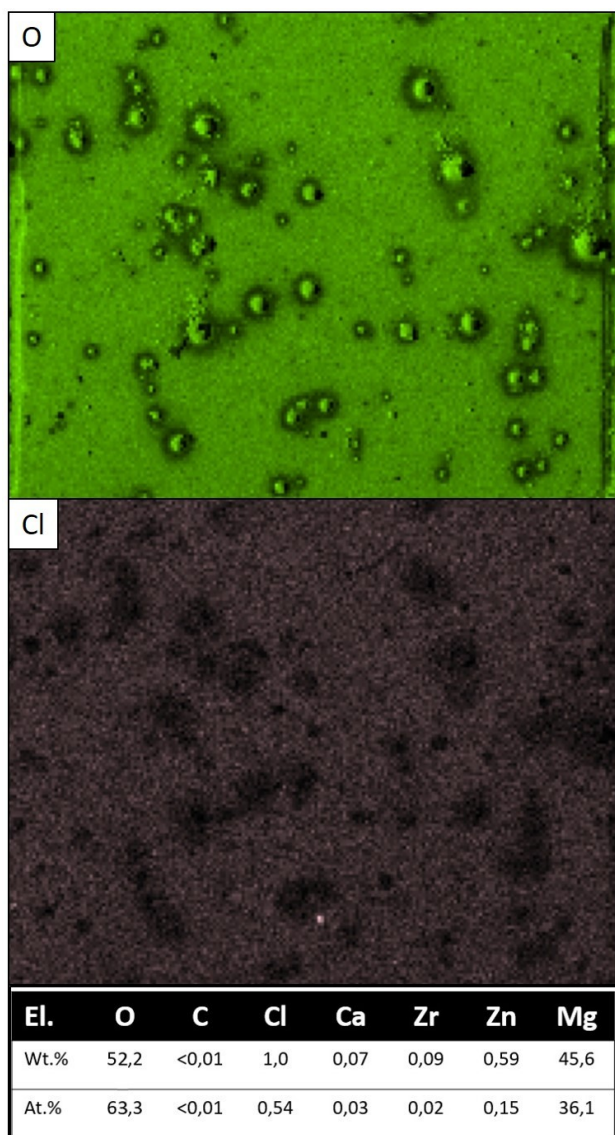


Fig. 8. Chemical composition and mapping of chlorine and oxygen in corrosion products on the marked surface of the EP-sample

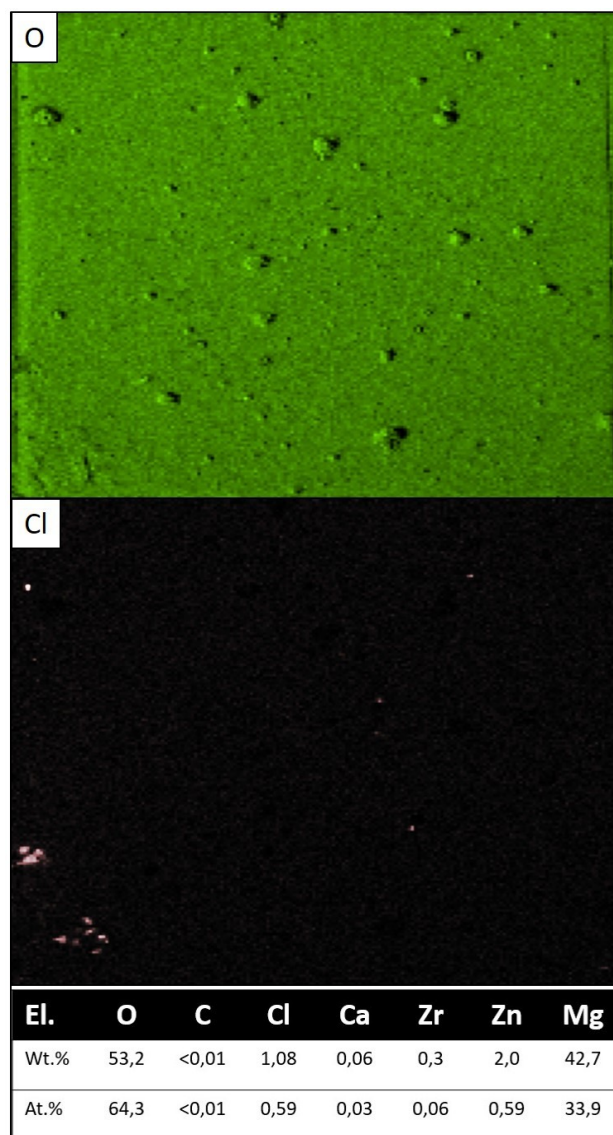


Fig. 9. Chemical composition and mapping of chlorine and oxygen in corrosion products on the marked surface of the pH-sample

The corrosion products of both samples consist mainly of magnesium hydroxide. The chlorine concentration is many times lower than the oxygen concentration. Most likely, this is a consequence of the magnesium chloride good solubility. There is very little carbon in the corrosion products, and it is located exclusively locally, sometimes adjoining calcium. Obviously, this is a consequence of the reaction of $Mg(OH)_2$ brucite and calcium hydroxide, with carbon dioxide from the air in these areas, resulting in the formation of magnesium carbonate [9; 19] and calcium carbonate.

Comparing the distribution of chemical elements and height maps, one can see that around the particles of inclusions and secondary phases of the EP sample, a large rounded zone is formed with a fairly clear boundary, the corrosion damage of which is much less than that of the surrounding material. It can be safely said that this zone reflects the distance at which the particle has a significant

effect on corrosion processes, and this distance is an order of magnitude greater than the size of the particle itself. This zone includes: a small centre, which is the particle itself and the material in the immediate proximity to it; the near halo, which is a wide rounded area with a distinct outer border in the form of a small elevation; the far halo, which is a wider rounded area between the near halo and the "outer" material, which is not affected by the processes caused by the particle in the centre. All three components of the zone of particle influence on the corrosion process are best seen in Fig. 6 and 10.

The chlorine content in corrosion products in the entire zone is many times less than in corrosion products in other places. The conclusion follows from this: the reaction described by equation (2) does not occur in this zone. This also explains its lesser damaging: chlorine does not destroy the passivating film of corrosion products. The oxygen content in the corrosion products in this zone shows its heterogeneity:

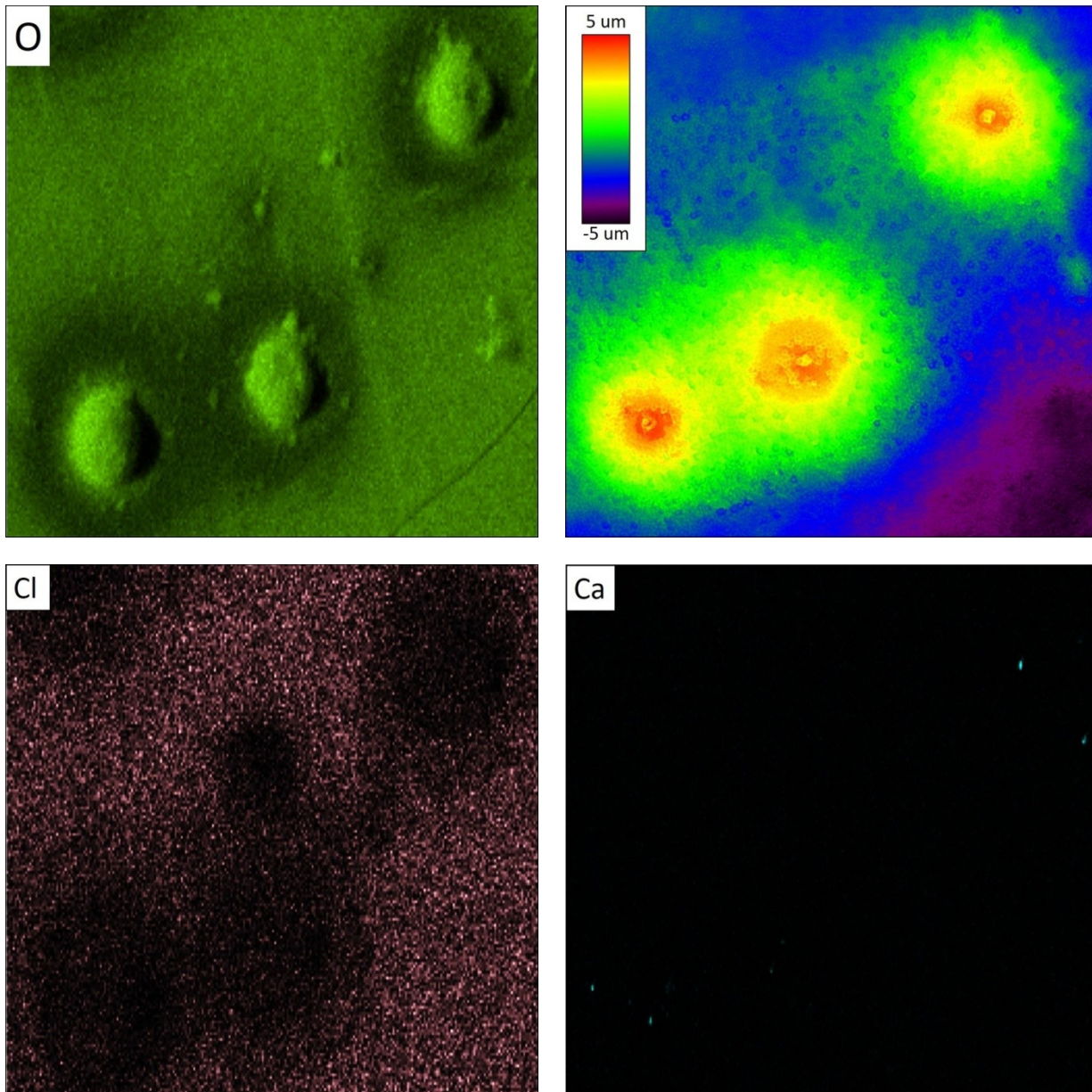
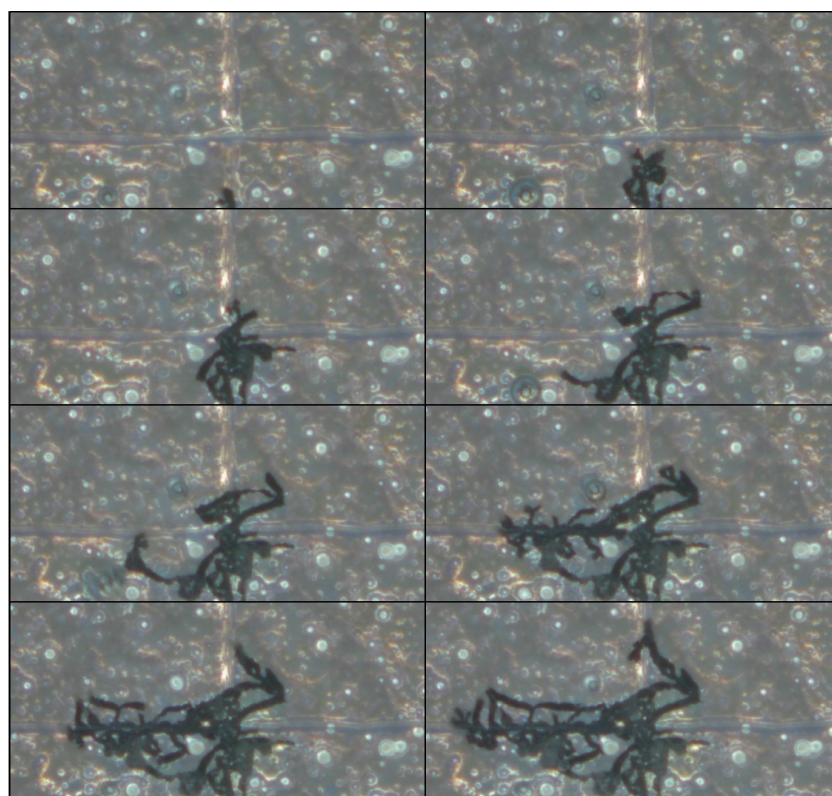


Fig. 10. Height map (after the removal of the corrosion products) and chemical elements mapping in the corrosion products on the area shown in Fig. 2

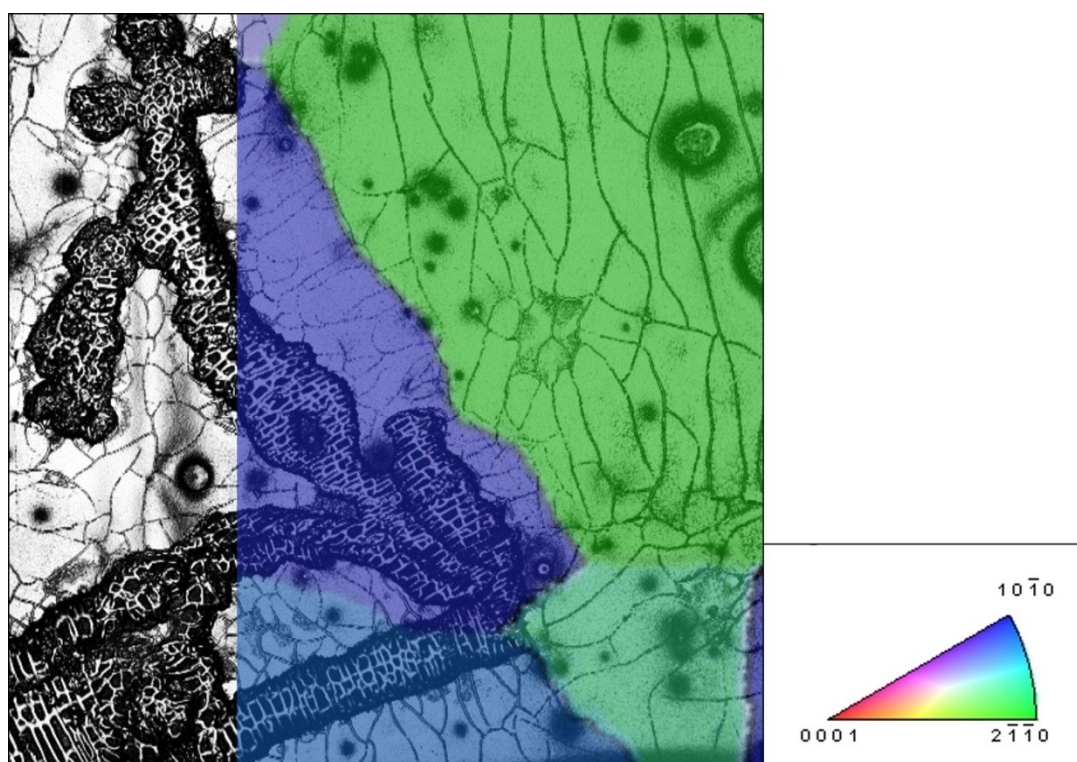
in the centre, and in the near halo it is approximately the same as in the corrosion products of the surrounding material, however, in the far halo, the oxygen concentration in the corrosion products drops sharply. At the same time, the height maps in Fig. 6 and 9 show that corrosion damage is present in the far halo and it is deeper than in the near halo. If the centre is the main corrosion point, then it is logically, to assume, that the pH level in the near-surface microvolumes of the corrosive medium will increase when approaching it. The Pourbaix diagram given in [10] follows that, at an electrode potential of -2.1 to -2.7 V and a high pH level, magnesium hydride and magnesium hydroxide are stable states in the Mg–H₂O electrochemical system. Thus, one can assume that in the centre and the near halo, as well as on the surface of the “outer” material, the reaction with the formation of brucite described by equation (1)

occurs, however, unlike the outer material, the resulting magnesium hydroxide is stable, and does not interact with chlorine, due to which its passivating properties are improved. In the far halo, the main corrosion product is presumably not hydroxide, but magnesium hydride, which could explain the very low oxygen concentration in the corrosion products at this location. Outside the zone of particle influence on corrosion processes, the reaction described by equation (1) is first performed, and then that described by equation (2); in this case, a uniform and continuous matrix dissolution occurs there.

In the case of the PH sample, this zone is much smaller and is limited to only ten microns around the particle, as can be seen in Fig. 6 and 9. No far halo is observed – the entire PH sample surface is uniformly covered with corrosion products containing an equal amount of oxygen.



a



b

*Fig. 11. Image of first type filiform corrosion of the sample to determine the pH (PH) influence: **a** – shooting sheet taken during corrosion tests (the period between frames is 4 minutes) showing the corrosion propagation speed and direction; **b** – optical image with IPF-map imposed on it*

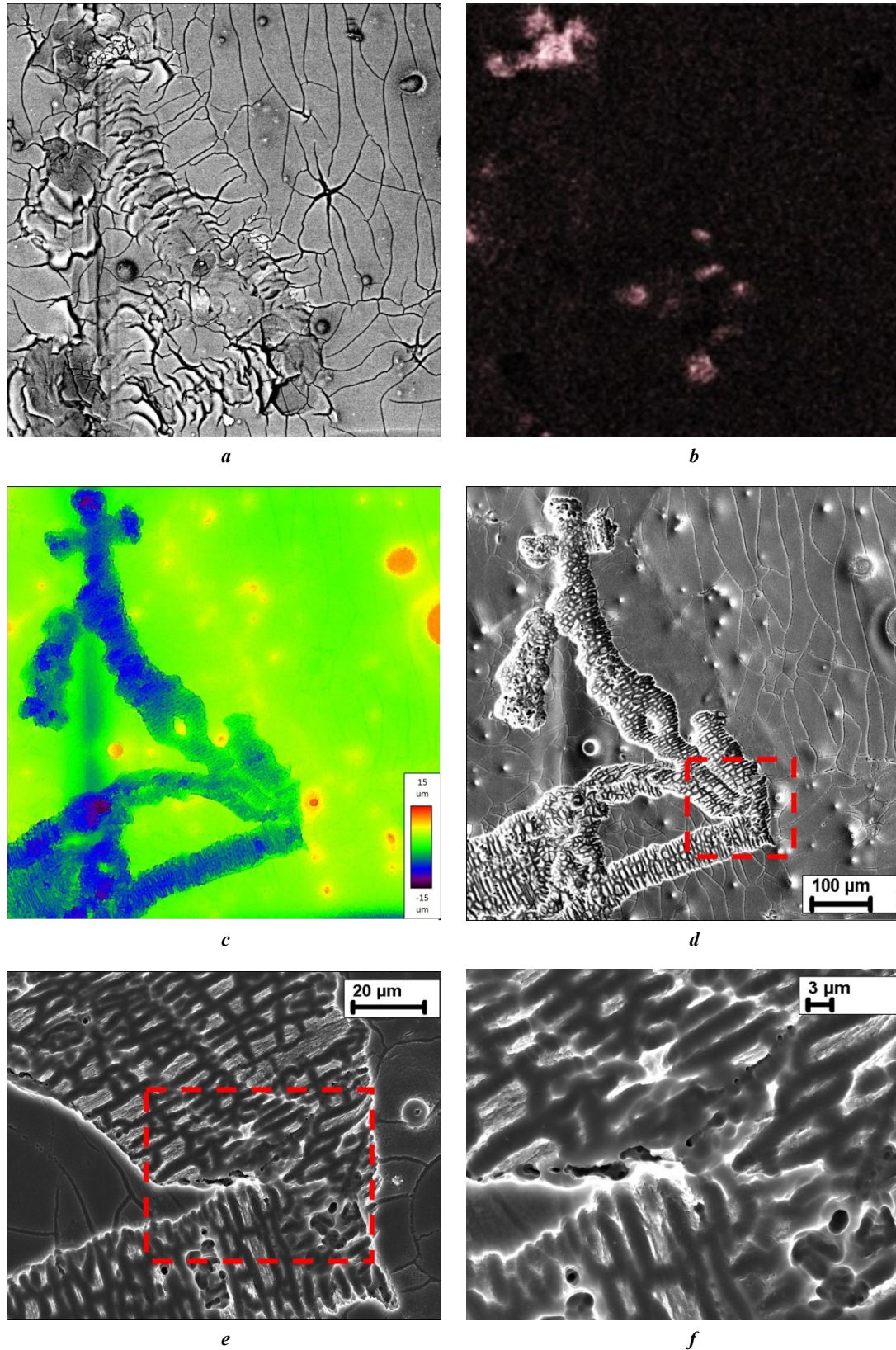


Fig. 12. Images of the first type filiform corrosion of the sample to determine the pH (PH) influence:
a – SEM image (bse-detector) before the removal of corrosion products; *b* – chlorine distribution in corrosion products;
c – height map after the removal of corrosion products; *d* – SEM-image; *e* – a fragment highlighted with a dotted line in Fig. 12 *d*;
f – a fragment highlighted with a dotted line in Fig. 12 *e*

Chlorine is evenly distributed in the corrosion products, except for several points of its increased concentration, primarily in the places of damages caused by the first type filiform corrosion. The height map shows the corrosion damage morphology, correlating with neither crystallography nor the composition of corrosion products, and therefore, is most likely determined by the trajectory of the flow washing the sample surface. Particles, and the small surface area around them, are also shown, on this map as higher and therefore less damaged areas. This may indicate that, at a small distance from the particle, the passivation effect manifests itself even under such conditions. It is curious that the corrosion damage morphology outside the marked area, to which the liquid flow was directed, is the same as in EP sample.

Fig. 2 and 10 show that the particle electrode potential had no effect on the eventual result of the corrosion process. This is easily explained by the fact that the formation of the above discussed area is conditioned by the pH level, which increases both during intense corrosion of the matrix metal, due to contact with more electropositive phases, and during the dissolution of electronegative phases, due to contact with a more positive matrix. One should note that for long-term tests, the difference might still appear, since the phases, more negative than magnesium, dissolve themselves. This means that their time of action is limited to the dissolution period – in contrast to the more noble phases, the electrochemical effect of which will remain until they will not be covered with a dense crust of corrosion products or simply will not precipitate from a corrosion-damaged surface.

Filiform corrosion traces of two types were observed on the surface of both samples. The first type is characterised by a wide (tens of microns) channel, high propagation velocity (up to hundreds of microns per minute), as well as by the fact that the channel originates in the places of scratches that marked the studied areas. Additional research showed that the scratches are free of contamination in the form of iron particles that could occur there with the chisel, their chemical composition is the same as that of the surrounding material, with the exception of the anomalous oxygen content. This indicates that the deformed scratch material is much more active than the surrounding material and is able to oxidise very quickly even upon air contact. The filiform corrosion second type is characterised by thin (1–2 μm) multiple channels over the entire sample surface. Now, nothing can be said about the places of its origin, and their propagation rate, since due to corrosion products, such light damages are invisible on video recording frames. Both types of filiform corrosion manifest themselves better on a PH sample, and both are closely related to crystallography. The first type changes the propagation direction depending on the grain crystallographic orientation, which is clearly seen in Fig. 11 b. The direction of the second type damage also depends on crystallography, as can be seen in Fig. 7 b.

The spread of the first type filiform corrosion proceeds as follows: a “corrosion front” – a corrosion centre of unknown origin, where, judging by the distribution map of chemical elements in corrosion products, there is a very high chlorine concentration, moves ahead. The “front” propagates both over scratches and over the base material, changing the movement direction depending on the crystal-

lographic orientation of the grains. Behind the “front”, deep rounded channel remains, which has a surface morphology in the form of rectangular honeycombs a few microns in size, oriented perpendicular to the main direction of the channel. In the corrosion products located in the channel, the amount of chlorine is the same as in the corrosion products of the base material, excluding some points where there was a change in the direction of filiform corrosion. Within this study, it is difficult to judge the nature of this phenomenon. Based on the fact, that chlorine practically does not remain at the points of damage, one can assume that the front is a moving centre, where the high-rate formation of chlorine-containing magnesium compounds and their prompt decay into ions that can participate in the reaction again take place. However, from the available information, it is not clear what these compounds are. Probably, this can be found out by the methods that allow determining not the elemental, but the phase composition of corrosion products, for example, infrared Fourier spectrometry.

CONCLUSIONS

1. During corrosion in an still (uncirculated) solution, a wide zone (many times larger than the particle itself) is formed around corrosion centres, which are particles of inclusions and secondary phases; this zone reflects an area, where corrosion processes depend on the particle. Corrosion damage in this zone is much less than in the rest of the material. This zone includes the centre, the near halo, and the far halo. These components have a clear boundary between themselves and with the surrounding material manifesting itself both in the difference in the damage depth and in the different composition of corrosion products. The latter means that different chemical reactions take place on the surface of the components of this zone, which is associated with the difference in the pH level.

2. The particle electrode potential does not have a visible effect on the formation of the aforementioned zone, which is probably associated as well with a stronger influence of the pH level.

3. When a sample is flowed over with a liquid removing a corrosive medium with a high pH content from the surface, the size of the round-shaped zone around the particle is many times smaller compared to the case when the sample is in a non-circulating solution.

4. Two types of filiform corrosion were identified: the first type forms damage in the form of a channel several tens of microns wide; the second type is 1–2 microns wide. The development of both types occurs in accordance with the crystallographic orientation of the grains. Corrosion of the first type originates in scratches, where the metal is more susceptible to oxidation.

REFERENCES

- Chen J., Tan L., Yu X., Etim I.P., Ibrahim M., Yang K. Mechanical properties of magnesium alloys for medical application: A review. *Journal of the Mechanical Behavior Biomedical Materials*, 2018, vol. 87, pp. 68–79. DOI: [10.1016/j.jmbbm.2018.07.022](https://doi.org/10.1016/j.jmbbm.2018.07.022).
- Vinogradov A., Merson E., Myagkikh P., Linderov M., Brilevsky A., Merson D. Attaining High Functional Performance in Biodegradable Mg-Alloys: An Overview of

- Challenges and Prospects for the Mg-Zn-Ca System. *Materials*, 2023, vol. 16, no. 3, article number 1324. DOI: [10.3390/ma16031324](https://doi.org/10.3390/ma16031324).
3. McCall C.R., Hill M.A., Lillard R.S. Crystallographic pitting in magnesium single crystals. *Corrosion Engineering Science and Technology*, 2005, vol. 40, no. 4, pp. 337–343. DOI: [10.1179/174327805X66326](https://doi.org/10.1179/174327805X66326).
 4. Shin K.S., Bian M.Z., Nam N.D. Effects of crystallographic orientation on corrosion behavior of magnesium single crystals. *JOM*, 2012, vol. 64, no. 6, pp. 664–670. DOI: [10.1007/s11837-012-0334-0](https://doi.org/10.1007/s11837-012-0334-0).
 5. Liu M., Qiu D., Zhao M.-C., Song G., Atrens A. The effect of crystallographic orientation on the active corrosion of pure magnesium. *Scripta Materialia*, 2008, vol. 58, no. 5, pp. 421–424. DOI: [10.1016/j.scriptamat.2007.10.027](https://doi.org/10.1016/j.scriptamat.2007.10.027).
 6. Bahl S., Suwas S., Chatterjee K. The control of crystallographic texture in the use of magnesium as a resorbable biomaterial. *RSC Advances*, 2014, vol. 4, no. 99, pp. 55677–55684. DOI: [10.1039/c4ra08484e](https://doi.org/10.1039/c4ra08484e).
 7. Ma Y., Wang D., Li H., Yuan F., Yang C., Zhang J. Microstructure, mechanical and corrosion properties of novel quaternary biodegradable extruded Mg-1Zn-0.2Ca-xAg alloys. *Materials Research Express*, 2020, vol. 7, no. 1, article number 015414. DOI: [10.1088/2053-1591/ab6a52](https://doi.org/10.1088/2053-1591/ab6a52).
 8. Parfenov E.V., Kulyasova O.B., Mukaeva V.R., Mingo B., Farrakhov R.G., Cherneikina Y.V., Erokhin A., Zheng Y.F., Valiev R.Z. Influence of ultra-fine grain structure on corrosion behaviour of biodegradable Mg-1Ca alloy. *Corrosion Science*, 2020, vol. 163, article number 108303. DOI: [10.1016/j.corsci.2019.108303](https://doi.org/10.1016/j.corsci.2019.108303).
 9. Thekkepat K., Han J.-S., Choi J.-W., Lee S.-Ch., Yoon E.S., Li G., Seok H.-H., Kim Y.-Ch., Kim J.-H., Cha P.-R. Computational design of Mg alloys with minimal galvanic corrosion. *Journal of Magnesium and Alloys*, 2022, vol. 10, no. 7, pp. 1972–1980. DOI: [10.1016/j.jma.2021.06.019](https://doi.org/10.1016/j.jma.2021.06.019).
 10. Song G.-L. Corrosion electrochemistry of magnesium (Mg) and its alloys. *Corrosion of Magnesium Alloys*, 2011, pp. 3–65. DOI: [10.1533/9780857091413.1.3](https://doi.org/10.1533/9780857091413.1.3).
 11. Salahshoor M., Guo Y. Biodegradable orthopedic magnesium-calcium (MgCa) alloys, processing, and corrosion performance. *Materials*, 2012, vol. 5, no. 1, pp. 135–155. DOI: [10.3390/ma5010135](https://doi.org/10.3390/ma5010135).
 12. Urwongse L., Sorrell C.A. The System MgO-MgCl₂-H₂O at 23°C. *Journal of American Ceramic Society*, 1980, vol. 63, no. 9-10, pp. 501–504. DOI: [10.1111/J.1151-2916.1980.TB10752.X](https://doi.org/10.1111/J.1151-2916.1980.TB10752.X).
 13. Merson D., Brilevsky A., Myagkikh P., Tarkova A., Prokhorikhin A., Kretov E., Frolova T., Vinogradov A. The functional properties of Mg-Zn-X biodegradable magnesium alloys. *Materials*, 2020, vol. 13, no. 3, article number 544. DOI: [10.3390/ma13030544](https://doi.org/10.3390/ma13030544).
 14. Merson D.L., Brilevsky A.I., Myagkikh P.N., Markushev M.V., Vinogradov A. Effect of deformation processing of the dilute Mg-1Zn-0.2Ca alloy on the mechanical properties and corrosion rate in a simulated body fluid. *Letters on Materials*, 2020, vol. 10, no. 2, pp. 217–222. DOI: [10.22226/2410-3535-2020-2-217-222](https://doi.org/10.22226/2410-3535-2020-2-217-222).
 15. Myagkikh P.N., Merson E.D., Poluyanov V.A., Merson D.L. Structure effect on the kinetics and staging of the corrosion process of biodegradable ZX10 and WZ31 magnesium alloys. *Frontier Materials & Technologies*, 2022, no. 2, pp. 63–73. DOI: [10.18323/2782-4039-2022-2-63-73](https://doi.org/10.18323/2782-4039-2022-2-63-73).
 16. McCall C.R., Hill M.A., Lillard R.S. Crystallographic pitting in magnesium single crystals. *Corrosion Engineering, Science and Technology*, 2005, vol. 40, no. 4, pp. 337–343. DOI: [10.1179/174327805X66326](https://doi.org/10.1179/174327805X66326).
 17. Zhang X., Wang Z., Yuan G., Xue Y. Improvement of mechanical properties and corrosion resistance of biodegradable Mg-Nd-Zn-Zr alloys by double extrusion. *Materials Science and Engineering: B*, 2012, vol. 177, no. 13, pp. 1113–1119. DOI: [10.1016/j.mseb.2012.05.020](https://doi.org/10.1016/j.mseb.2012.05.020).
 18. Ding Y., Wen C., Hodgson P., Li Y. Effects of alloying elements on the corrosion behavior and biocompatibility of biodegradable magnesium alloys: A review. *Journal of Materials Chemistry B*, 2014, vol. 2, no. 14, pp. 1912–1933. DOI: [10.1039/c3tb21746a](https://doi.org/10.1039/c3tb21746a).
 19. Yang Y., He C., Dianyu E., Yang W., Qi F., Xie D., Shen L., Peng S., Shuai C. Mg bone implant: Features, developments and perspectives. *Materials and Design*, 2020, vol. 185, article number 108259. DOI: [10.1016/j.matdes.2019.108259](https://doi.org/10.1016/j.matdes.2019.108259).
 20. Esmaily M., Svensson J.E., Fajardo S., Birbilis N., Frankel G.S., Virtanen S., Arrabal R., Thomas S., Johansson L.G. Fundamentals and advances in magnesium alloy corrosion. *Progress in Materials Science*, 2017, vol. 89, pp. 92–193. DOI: [10.1016/j.pmatsci.2017.04.011](https://doi.org/10.1016/j.pmatsci.2017.04.011).